A new rigid-viscoplastic model for simulating thermal strain effects in metal forming processes

Eduardo N. Dvorkin and Rita G. Toscano
Center for Industrial Research, FUDETEC
Av. Córdoba 320
1054, Buenos Aires, Argentina

Abstract

A new rigid-viscoplastic model that includes the effect of thermal strains when modeling steady state metal forming processes was developed. A symmetric approximation to the resulting non-symmetric stiffness matrix was derived.The thermo-mechanical flow formulation was implemented using the pseudo-concentrations technique.The new formulation was numerically tested showing that it provides reliable results.

1 Introduction

During hot metal forming processes the non-homogeneous thermal evolution of the workpiece produces differential thermal expansions in the processed material. These thermal strains are enhanced by the phase transformations that take place at elevated temperatures.

In Figs. 1 and 2 we present the dilatometries corresponding to two low alloyed steels under different cooling conditions, both dilatometries were obtained during continuous cooling transformation tests. In the first case the steel undergoes a martensitic transformation (quenching) and in the second case the steel transforms from austenite to ferrite / perlite.

As an example of metal forming processes in which the thermal strains play a fundamental role we may refer to the continuous casting processes, where the outer part of the solidifying strand cools faster than the inner part, inducing therefore differential thermal strains in the strand. These thermal strains are enhanced due to the liquid-solid transformation and due to the solid state phase transformations that take place at temperatures below solidus; the differential thermal strains may induce crack formation inside the solidifying strand [1]. In other processes such as hot rolling, quenching, etc. there are also non-homogeneous temperature evolutions that induce high stresses which may damage the processed material.

The non-homogeneous thermal strains inside the workpiece, which include the transformation induced strains, need to be adequately controlled during

metal forming processes. Therefore it is very important that when numerically simulating hot metal forming processes to investigate their *technological windows* [2], we properly include in the models the effect of the thermal strains.

The modeling of coupled thermo-mechanical metal forming processes has been discussed in a number of publications, among them we can refer to Refs. [3] - [8].

In the case of the metal forming simulations developed using the flow formulation [9] (rigid-viscoplastic material models [10]) the developments available in the literature only include for the thermo-mechanical coupling:

- In the energy balance equations, the term that accounts for the heat generated by the viscoplastic dissipation.
- In the momentum balance equations, the temperature dependence of the material properties.

In all cases the thermal strains are neglected.

In the second section of this paper we discuss the inclusion of thermal strains in the flow formulation, focusing our discussion on steady state analyses. In the third section we comment on the implementation of our formulation via the pseudo-concentrations technique [11] - [18].

To investigate the performance of the developed thermo-mechanical formulation in the fourth section of this paper we discuss selected numerical examples.

2 Inclusion of thermal strains in the flow formulation

For the rigid-viscoplastic material constitutive relation that is used in the flow formulation we decompose the total strain rate into its viscoplastic and thermal components,

$$\dot{\varepsilon}_{ij} = \dot{\varepsilon}^{VP}_{ij} + \dot{\varepsilon}^{TH}_{ij} \tag{1a}$$

$$\dot{\varepsilon}^{TH}_{ij} = \frac{D(\alpha T)}{Dt}\,\delta_{ij}\ . \tag{1b}$$

In Eqn. (1b) we use the notation $\frac{D(\cdot)}{Dt}$ to indicate the material time derivative, that is to say, we keep constant the material particle when we calculate the time derivative [19]. Also α is the total expansion coefficient, function of the material temperature, T.

Using the standard expression for calculating the material time derivative [19] we get,

$$\frac{D(\alpha T)}{Dt} = \frac{\partial(\alpha T)}{\partial t} + \underline{v}\cdot\underline{\nabla}(\alpha T)\ , \tag{2}$$

where $\underline{v}$ is the material velocity.

Hence, for a steady-state problem, we can write Eqn. (1a) as,

$$\dot{\varepsilon}_{ij} = \dot{\varepsilon}^{VP}_{ij} + \underline{v} \cdot \underline{\nabla}(\alpha T)\, \delta_{ij} \ . \tag{3}$$

For modeling metal forming processes we use an associated von Mises viscoplastic constitutive relation. The incompressibility of the associated von Mises viscoplastic flow [10] is expressed as,

$$\dot{\varepsilon}^{VP}_{v} = \dot{\varepsilon}^{VP}_{ij}\, \delta_{ij} = 0 \ . \tag{4}$$

For this relation we define the equivalent viscoplastic strain rate as [10],

$$\dot{\overline{\varepsilon}}^{VP} = (\frac{2}{3}\, \dot{\varepsilon}^{VP}_{ij}\ \dot{\varepsilon}^{VP}_{ij}\ )^{\frac{1}{2}} \ . \tag{5}$$

To describe the material hardening we use the Fields-Backofen hardening model, [20] [21],

$$\sigma_y = \sigma_o(T)\ \left(\overline{\varepsilon}^{VP}\right)^n \left(\dot{\overline{\varepsilon}}^{VP}\right)^m \tag{6}$$

where the total equivalent viscoplastic strain ($\overline{\varepsilon}^{VP}$) is obtained from [13],

$$\dot{\overline{\varepsilon}}^{VP} = \frac{\partial\, \overline{\varepsilon}^{VP}}{\partial\, t} + \underline{v} \cdot \underline{\nabla}\overline{\varepsilon}^{VP} \ . \tag{7}$$

Hence, we get [9]

$$s_{ij} = 2\,\mu \left[\dot{\varepsilon}^{VP}_{ij}\right]' \tag{8a}$$

$$\mu = \frac{1}{3}\frac{\sigma_o(T)\ \left(\overline{\varepsilon}^{VP}\right)^n}{\left(\dot{\overline{\varepsilon}}^{VP}\right)^{(1-m)}} \ . \tag{8b}$$

In the above equations s_{ij} are the deviatoric components of the Cauchy stress tensor (σ_{ij}) and $\left[\dot{\varepsilon}^{VP}_{ij}\right]'$ are the deviatoric components of the viscoplastic strain rate tensor.

It is important to consider that during solid phase transformations the yield stress has to be determined using, in a weighted average, the yield stress of each phase and also taking into account the phenomenon of transformation plasticity which is discussed in Refs. [22] and [23].

For solving a steady state problem we start from a trial equilibrium configuration and we calculate its corresponding velocity field via the Principle of Virtual Power; since the velocity field has to fulfill the incompressibility constraint in Eqn. (4) we impose it using an augmented Lagrangian technique [14],

[24]. Once the equilibrium velocity field is calculated, the assumed equilibrium configuration is modified using the staggered iterative procedure that we are going to discuss in the next section.

The solution of the material nonlinearities (8b) together with the augmented Lagrangian technique produce an iterative system of equations.

For the "$k+1$" iteration we get,

$$\int_V s_{ij}^{(k+1)}\ \delta\left[\dot{\varepsilon}_{ij}\right]'\ dv + \int_V p^{(k+1)}\ \delta\dot{\varepsilon}_v dv = \mathcal{R}\ . \tag{9}$$

The term on the r.h.s., $\mathcal{R}$, is the virtual power of the external loads and,

$$\begin{aligned}
\underline{\boldsymbol{x}}^{(k+1)} &= \underline{\boldsymbol{x}}^{(k)} + \Delta\underline{\boldsymbol{x}}^{(k+1)} && (10a)\\
\delta\underline{\boldsymbol{v}} &= \delta\ \Delta\underline{\boldsymbol{v}}^{(k+1)} && (10b)\\
\dot{\varepsilon}_{ij}^{(k+1)} &= \dot{\varepsilon}_{ij}^{(k)} + \Delta\dot{\varepsilon}_{ij}^{(k+1)} && (10c)\\
s_{ij}^{(k+1)} &= 2\left[\mu\dot{\varepsilon}'_{ij}\right]^{(k+1)} && (10d)\\
\delta\dot{\varepsilon}_{ij} &= \delta\ \Delta\dot{\varepsilon}_{ij}^{(k+1)}\ . && (10e)
\end{aligned}$$

The pressure field is calculated using the augmented Lagrangian technique [24],

$$p^{(k+1)} = p^{(k)} + \kappa\left[\dot{\varepsilon}_v^{VP}\right]^{(k+1)} = p^{(k)} + \kappa\left[\dot{\varepsilon}_v^{VP}\right]^{(k)} + \kappa\left[\Delta\dot{\varepsilon}_v^{VP}\right]^{(k+1)}\ . \tag{11}$$

In the above κ is the penalty coefficient used with the augmented Lagrangian technique to impose incompressibility. A discussion on its adequate selection was presented in Ref. [14].

Also, from the strain rate decomposition in Eqn. (1a) we get,

$$\begin{aligned}
\left[\dot{\varepsilon}_{ij}^{VP}\right]^{(k)} &= \dot{\varepsilon}_{ij}^{(k)} - \left[\dot{\varepsilon}_{ij}^{TH}\right]^{(k)} && (12a)\\
\left[\Delta\dot{\varepsilon}_{ij}^{VP}\right]^{(k)} &= \Delta\dot{\varepsilon}_{ij}^{(k)} - \left[\Delta\dot{\varepsilon}_{ij}^{TH}\right]^{(k)}\ . && (12b)
\end{aligned}$$

For a steady state problem, and assuming that the temperature field is known we get from Eqn. (3),

$$\begin{aligned}
\dot{\varepsilon}_v^{TH} &= 3\underline{\boldsymbol{v}}\cdot\underline{\nabla}\left(\alpha T\right) && (13a)\\
\Delta\dot{\varepsilon}_v^{TH} &= 3\ \Delta\underline{\boldsymbol{v}}\cdot\underline{\nabla}\left(\alpha T\right)\ . && (13b)
\end{aligned}$$

We now introduce the finite element method using a three field interpolation [14] ; hence, we get

$$\left[\int_V \underline{B}_D^T \ (2\mu)^{(k)} \ \underline{B}_D \ dv + \int_V \underline{B}_V^T \ \kappa \ \underline{B}_V \ dv - 3 \int_V \underline{B}_V^T \ \kappa \ \underline{C} dv\right] \ \Delta \dot{\underline{U}}^{(k+1)} \tag{14}$$
$$= \underline{R} - \int_V \underline{B}_D^T \ \underline{S}^{(k)} \ dv - \int_V \underline{B}_V^T \ (\underline{P}^{(k)} + \kappa \ \left[\dot{\varepsilon}_v^{VP}\right]^{(k)}) \ dv \ .$$

In the above equation $\underline{R}$ is the nodal vector equivalent (in the virtual work sense) to the external loads acting on the body. Also at any point inside an element,

$$\underline{S} = \begin{bmatrix} s_{11} \\ s_{22} \\ s_{33} \\ s_{12} \\ s_{23} \\ s_{31} \end{bmatrix} \ . \tag{15}$$

The vector $\underline{P}$, contains the terms that define the pressure field inside each element.

The interpolations used above are discussed in Ref. [14]; being $\dot{\underline{U}}$ the vector of nodal velocities, we can write

$$\left[\Delta \dot{\underline{\varepsilon}}'\right]^{(k+1)} = \underline{B}_D \ \Delta \dot{\underline{U}}^{(k+1)} \tag{16a}$$
$$\left[\Delta \dot{\underline{\varepsilon}}_v\right]^{(k+1)} = \underline{B}_V \ \Delta \dot{\underline{U}}^{(k+1)} \ . \tag{16b}$$

At any point inside an element the components of $\dot{\varepsilon}'_{ij}$ and $\dot{\varepsilon}_v$ are ordered in the column arrays $\dot{\underline{\varepsilon}}'$ and $\dot{\underline{\varepsilon}}_v$ respectively.

The last term inside the bracket on the l.h.s. of Eqn. (14) comes from,

$$\int_V \delta \dot{\varepsilon}_V \kappa \ 3 \ \Delta \underline{v} \cdot \underline{\nabla} (\alpha T) \ dv \ .$$

In the H1-P0 hexahedral element [14] we calculate the term, $[\Delta \underline{v} \cdot \underline{\nabla} (\alpha T)]$, at the element center and then we interpolate it as a constant over the element volume; hence,

$$\underline{C} = \left[- - - - - - |\nabla (\alpha T)|_1^O \ h_k^O \quad |\nabla (\alpha T)|_2^O \ h_k^O \quad |\nabla (\alpha T)|_3^O \ h_k^O \ - - - - - -\right] \ . \tag{17}$$

In the above equation we have written in detail the $C-$components corresponding to the node "k". Also, $|\cdot|^O$ indicates that the quantity within the bars is calculated at the element center and $[\cdot]_i$ is the $i-th$ component of a vector.

The term $\left[3\int_V \underline{B}_V^T\,\kappa\,\underline{C} dv\right]$ adds a non-symmetric component to the stiffness matrix.

2.1 A symmetric formulation

For implementing the above developed formulation in an existing finite element code it is usually preferred to work with symmetric matrices, even if convergence may be slower.

Usual brute-force symmetrization procedures such as, preserving on the l.h.s. of Eqns. (14) only the symmetric part of $\left[3\int_V \underline{B}_V^T\,\kappa\,\underline{C}\,dv\right]$ or sending the term $\left[3\int_V \underline{B}_V^T\,\kappa\,\underline{C}\,dv\right]$ to the r.h.s. with its value calculated from the velocity field obtained in the previous iteration, did not converge in our numerical tests.

For symmetrizing the stiffness matrix we introduce the following assumption:

$$\Delta\dot{\varepsilon}_v^{TH} = \frac{\left[\dot{\varepsilon}_v^{TH}\right]^{(k)}}{\left[\dot{\varepsilon}_v\right]^{(k)}}\,\Delta\dot{\varepsilon}_v\ . \tag{18}$$

Hence, we can use instead of the non-symmetric term $\left[3\int_V \underline{B}_V^T\,\kappa\,\underline{C}\,dv\right]$ the symmetric one,

$$\Delta\underline{K} = \int_V \underline{B}_V^T\,\kappa\,\frac{\left[\dot{\varepsilon}_v^{TH}\right]^{(k)}}{\left[\dot{\varepsilon}_v\right]^{(k)}}\,\underline{B}_V\,dv\ . \tag{19}$$

Our numerical experimentation has shown that when using the above procedure the iterative method converges in a reasonable number of iterations.

3 Implementation via the pseudo-concentrations technique

In previous references we implemented the flow formulation using an Eulerian description of motion, via Thompson's pseudo-concentrations technique [11] - [18] and [7].

We use a fixed mesh with the material moving inside it; at each point interior to the mesh we define a variable named *pseudo - concentration* (c):

$c \geqslant 0 \Longleftrightarrow$ there is material at the point,
$c < 0 \Longleftrightarrow$ there is no material at the point.

At the points where $c < 0$ we use a very low viscosity (not zero to avoid a singular siffness matrix) and $\alpha = 0$.

In previous applications of the pseudo-concentrations technique we have dealt with incompressible problems; however, in the present case the material density (ρ) rather than being constant is a function of the temperature: $\rho = \rho(T)$. We can write the mass conservation principle as [19],

$$\frac{\partial \rho}{\partial t} + \underline{\nabla} \cdot (\rho \, \underline{v}) = 0 \, . \tag{20}$$

We now define the concentration as concentration per unit mass and its conservation equation is,

$$\frac{\partial (\rho c)}{\partial t} + \underline{\nabla} \cdot (\rho \, c \, \underline{v}) = 0 \, . \tag{21}$$

Using together Eqns. (20) and (21) we get,

$$\underline{v} \cdot \underline{\nabla} c = 0 \quad (stationary\ problems) \tag{22a}$$

$$\frac{\partial c}{\partial t} + \underline{v} \cdot \underline{\nabla} c = 0 \quad (transient\ problems) \tag{22b}$$

Some notes regarding our Eulerian formulation based on the pseudo-concentrations technique:

- It provides the free surfaces in stationary and transient problems without any special free surface algorithm.
- It does not require a remeshing algorithm, usually needed when using Lagrangian or ALE formulations.

For the complete mesh we can re-write Eqn. (7) as,

$$\underline{v} \cdot \underline{\nabla} \overline{\varepsilon}^{VP} = \frac{\langle c \rangle}{|c|} \dot{\overline{\varepsilon}}^{VP} \quad (stationary\ problems) \tag{23a}$$

$$\frac{\partial \overline{\varepsilon}^{VP}}{\partial t} + \underline{v} \cdot \underline{\nabla} \overline{\varepsilon}^{VP} = \frac{\langle c \rangle}{|c|} \dot{\overline{\varepsilon}}^{VP} \quad (transient\ problems) \, . \tag{23b}$$

In the above, $\langle \cdot \rangle$ is a Macauley bracket.

A staggered iterative scheme was implemented to couple the equilibrium equations to the c-transport and $\overline{\varepsilon}$-transport equations.

For stationary problems we start the iterative algorithm from a trial c-distribution and zero trial velocities, except at those points where the velocities are prescribed as boundary conditions; hence we start with a trial velocity field $\widehat{\underline{v}}$.

1. $l = -1$
2. $l = l + 1$
   (i) $j = 0$; $\underline{v}^{(j)} = \widehat{\underline{v}}$
   (ii) $j = j + 1$
   Solve the workpiece nonlinear equilibrium equations keeping constant the c-distribution and the $\overline{\varepsilon}$-distribution (Eqns. (9)- (10e))
   $\underline{v}^{(j)} = f\,(\,\underline{v}^{(j-1)},\, c^{(l)},\, \overline{\varepsilon}^{(l)})$
   (iii) $IF\ \frac{\|\underline{v}^{(j)} - \underline{v}^{(j-1)}\|_2}{\|\underline{v}^{(j)}\|_2} \leq UTOL\ .AND.\ \left\| \dot{\varepsilon}_v^{VP} \right\|_\infty \leq VTOL$
   $THEN \longrightarrow \underline{v}^{(l)} = \underline{v}^{(j)} GO\ TO\ 3$
   $ELSE \longrightarrow GO\ TO$ 2.(ii)
3. *Calculate the c-distribution and $\overline{\varepsilon}$-distribution integrating (22a) and (23a) using the SUPG technique [25]*
4. $IF\ l = 0\ GO\ TO$ 2
   $ELSE \longrightarrow IF \frac{\|\underline{v}^{(l)} - \underline{v}^{(l-1)}\|_2}{\|\underline{v}^{(l)}\|_2} \leq UTOL$
   $THEN \longrightarrow CONVERGENCE$
   $ELSE \longrightarrow GO\ TO$ 2

Box I: Staggered iterative algorithm for coupling the equilibrium equations to the c−transport and $\overline{\varepsilon}$-transport equations.

When using the pseudo-concentrations technique, the coupling between the thermal and mechanical models is performed as discussed in Ref. [7].

4 Numerical experimentation

In this section we are going to discuss the numerical results that we obtained when solving selected steady state problems, using the developed thermo-mechanical formulation, implemented in our computer code METFOR.

4.1 Flow through a constant section duct under a thermal gradient

In this example we investigate the steady state flow through a constant square section duct with frictionless walls. We assume that the material flowing through the duct is subjected to a constant axial thermal gradient.

The material properties (6) are,

$$\begin{aligned} \sigma_o(T) &= 229.41\ \exp(-0.0029T) \\ n &= 0.2520 \\ m &= 0.1430 \\ \alpha &= 0.00002 \end{aligned}$$

and the axial temperature gradient is,

$$\frac{\partial T}{\partial x} = 500 \ .$$

The analytical solution is for the average velocity at each section,

$$v(x) = v(0) \ \exp(3\alpha \frac{\partial T}{\partial x} x) \ .$$

In Fig. 3 we compare the finite element and analytical solutions, obtaining a perfect match.

4.2 Flow through a nozzle under a thermal gradient

In this example we discuss the plane strain, steady state flow of a material through a convergent nozzle with frictionless walls. Again we assume that the material flowing through the duct is subjected to a constant axial thermal gradient and we use the same material parameters as in the previous example.

In Fig. 4 we show the finite element mesh that we used to analyze this example and in Fig. 5 we compare the average axial velocity for each section, calculated with METFOR and with an analytical solution. Again both solutions present an excellent agreement.

4.3 Plane strain plate

We consider a square plate free to expand in its plane and subjected to a plane strain state, under a constant temperature gradient along the horizontal side,

$$\frac{\partial T}{\partial x} = 500 \ .$$

Material properties:

$$\begin{aligned} \sigma_o &= 3.00 \\ n &= 0 \\ m &= 1 \\ \alpha &= 0.0002 \ . \end{aligned}$$

We are going to compare for this example two solutions:

- An Eulerian solution obtained using the thermo-mechanical formulation that we developed above.
- A Lagrangian solution obtained using a thermo-elastic large strains formulation in which:

$$ {}^{t}_{0}H^{TH}_{ij} = \alpha({}^{t}T - {}^{0}T)\ \delta_{ij} \quad . $$

The ${}^{t}_{0}H^{TH}_{ij}$ are the Hencky (logarithmic) thermal strains calculated for a temperature distribution given by ${}^{t}T(x, y)$ and referred to a state with a constant ${}^{0}T$ temperature. The elastic response of the material was modeled as almost incompressible.

In Fig. 6 we present the results of the Eulerian analysis in terms of pseudo-concentrations distribution.

In Figs. 7 and 8 we compare the analytical and Lagrangian solutions with the Eulerian solutions obtained using meshes with increasing refinement in the vertical direction; the comparison shows that the new formulation produces very good results.

4.4 Three-dimensional expansion

In this case we analyze the flow of a material under a constant axial thermal gradient; the material is free to expand in every direction. The constitutive properties are the same as the ones considered in the previous case.

In Fig. 9 we display the resulting pseudo-concentrations distribution that we get using the developed formulation; the rounded corners are due to the numerical diffusion introduced when solving the transport equation (22a). In Fig. 10 we present the resulting volumetric flow compared with the volumetric flow calculated using an analytical solution.

5 Conclusions

A new rigid-viscoplastic model that includes the effect of thermal strains when modeling steady state metal forming processes was developed. A symmetric approximation to the resulting non-symmetric stiffness matrix was derived.

The new formulation expands the applicability of the rigid-viscoplastic material models, since the alternative for simulating the effect of thermal strains in metal forming models is to introduce the elastic effects into the model, with the corresponding increase in computational times.

The thermo-mechanical flow formulation was implemented using the pseudo-concentrations technique.

The new formulation was numerically tested in simple problems showing that it provides reliable results. The next step will be to use it for the solution of involved industrial models of manufacturing processes (e.g. continuous casting of steel slabs, hot rolling, etc.); for those cases it will be fundamental to have as input to the model reliable data of mechanical material properties as a function of temperature [26].

Acknowledgment. *We gratefully acknowledge the support of the Techint Steel Sector for this research.*

References

[1] J.K.Brimacombe and K.Sorimachi, "Crack formation in the continuous casting of steel", *Metallurgical Transactions B*, **8B**, pp.489 - 505, 1977.

[2] E.N.Dvorkin, "Computational modelling for the steel industry at CINI", *IACM-Expressions*, N°10, 2001.

[3] N.Rebelo and S.Kobayashi, "A coupled analysis of viscoplastic deformation and heat transfer - I", *Int. J. Mech. Sci.,* **22**, pp.699-705, 1980.

[4] O.C.Zienkiewicz, E.Oñate and J.C.Heinrich, "A general formulation for coupled thermal flow of metals using finite elements", *Int .J. for Num. Methods in Engng.*, **17**, pp.1497-1514, 1981.

[5] S.Kobayashi, "Thermoviscoplastic analysis of metal forming problems by the finite element method", *Numerical Analysis of Forming Processes,* (Ed. J.F.T.Pittman et al), John Wiley & Sons, 1984.

[6] S.Kobayashi, S.-I.Oh and T.Altan, *Metal Forming and the Finite Element Method*, Oxford University Press, 1989.

[7] M.A.Cavaliere, M.B.Goldschmit and E.N.Dvorkin, "On the solution of coupled thermo-mechanical problems via the pseudo-concentrations technique" , *Proceedings ECCOMAS 2000 (European Congress on Computational Methods in Applied Sciences and Engineering) - COMPLAS VI (Sixth Int. Conf. on Computational Plasticity)*, CIMNE, Barcelona, 2000.

[8] R.H.Wagoner and J.-L.Chenot, *Metal Forming Analysis*, Cambridge University Press, 2001.

[9] O.C.Zienkiewicz, P.C.Jain and E.Oñate, "Flow of solids during forming and extrusion: some aspects of numerical solutions", *Int.J.Solid Struct.*, **14**, pp.15-28, 1977.

[10] P.Perzyna, "Fundamental problems in viscoplasticity", *Advances in Applied Mechanics*, **9**, Academic Press, 1966.

[11] E.Thompson, "Use of the pseudo-concentrations to follow creeping viscous flows during transient analysis", *Int. J. for Num. Methods in Fluids*, **6**, pp.749-761, 1986.

[12] E.Thompson and R.E.Smelser, "Transient analysis of forging operations by the pseudo-concentrations method",*Int .J. for Num. Methods in Engng. ,* **25**, pp.177-189, 1988.

[13] E.N.Dvorkin and E.G.Petöcz, "An effective technique for modelling 2D metal forming processes using an Eulerian formulation", *Engrg. Comput.*, **10**, pp.323-336, 1993.

[14] E.N.Dvorkin, M.A.Cavaliere and M.B.Goldschmit, "A three field element via augmented Lagrangian for modelling bulk metal forming processes", *Comput. Mechs.*, **17**, pp.2-9, 1995.

[15] E.N.Dvorkin, M.B.Goldschmit, M.A.Cavaliere, P.M.Amenta, O.Marini and W.Stroppiana, "2D finite element parametric studies of the flat rolling process", *J. of Materials Processing Technology*, **68**, pp.99-107, 1997.

[16] E.N.Dvorkin, M.A.Cavaliere, M.B.Goldschmit and P.M.Amenta, "On the modeling of steel product rolling processes", *Int.J.Forming Processes (ESAFORM)*, **1**, pp.211-242, 1998.

[17] M.A.Cavaliere, M.B.Goldschmit and E.N.Dvorkin, "Finite element analysis of steel rolling processes", *Computers & Structures*, **79**, pp.2075-2089, 2001.

[18] M.A.Cavaliere, M.B.Goldschmit and E.N.Dvorkin, "Finite element simulation of the steel plates hot rolling process", *Int. J. Numerical Methods in Engng.*, **52**, pp.1411-1430, 2001.

[19] L.E.Malvern, *Introduction to the Mechanics of a Continuous Medium*, Prentice-Hall, Englewood Cliffs, NJ, 1969.

[20] D.S.Fields and W.A.Backofen, "Determination of strain hardening characteristics by torsion testing", *Proc. ASTM,* **57**, pp.1259-1271, 1957.

[21] W.A.Backofen, *Deformation Processing*, Addison-Wesley, Reading MA, 1972.

[22] F.G.Rammerstorfer, D.F.Fischer, W.Mitter, K.J.Bathe and M.D.Snyder, "On thermo-elastic-plastic analysis of heat-treatment processes including creep and phase changes", *Computers & Structures*, **13**, pp.771-779, 1981.

[23] A.J.Fletcher, *Thermal Stresses and Strain Generation in Heat Treatment*, Elsevier Applied Science, 1989.

[24] D.G.Luenberger, *Linear and Nonlinear Programming*, Addison-Weley, 1984.

[25] T.J.R.Hughes, *The Finite Element Method*, Prentice-Hall, 1987.

[26] E.N.Dvorkin, M.A.Cavaliere and M.B.Goldschmit, "Finite element models in the steel industry. Part I: simulation of flat product manufacturing processes", *Computers & Structures*, (in press)

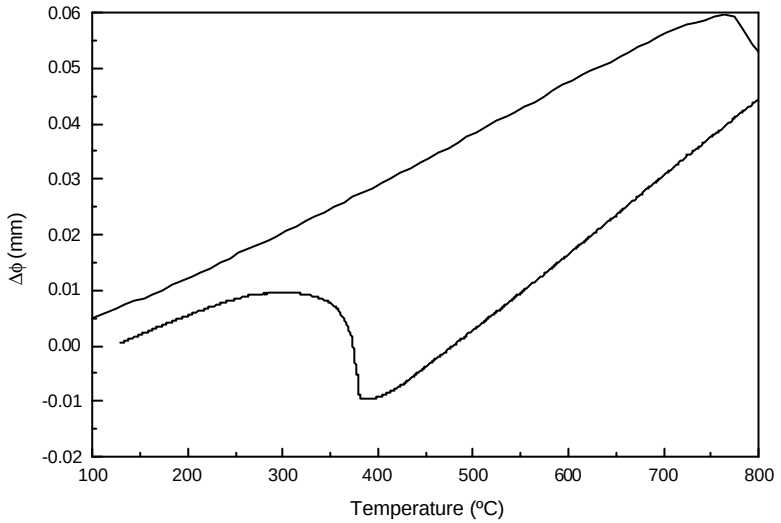

Figure 1: Dilatometry of a steel showing a martensitic transformation when cooling

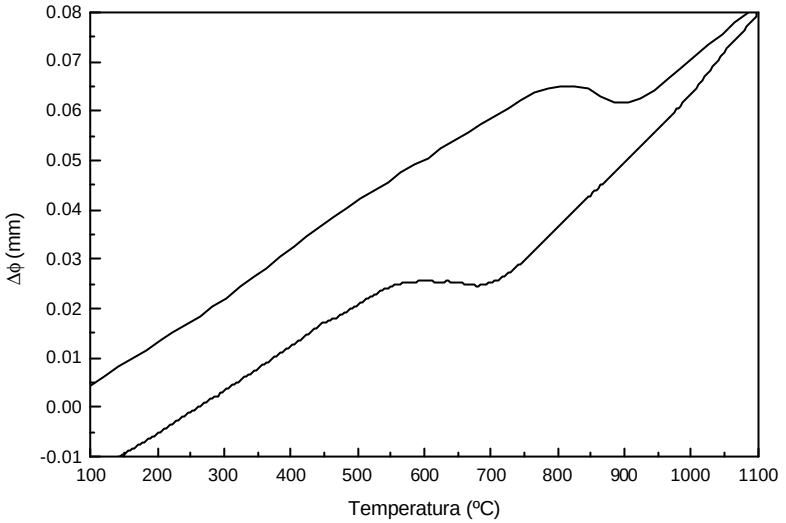

Figure 2: Dilatometry of a steel showing a diffusional transformation when cooling

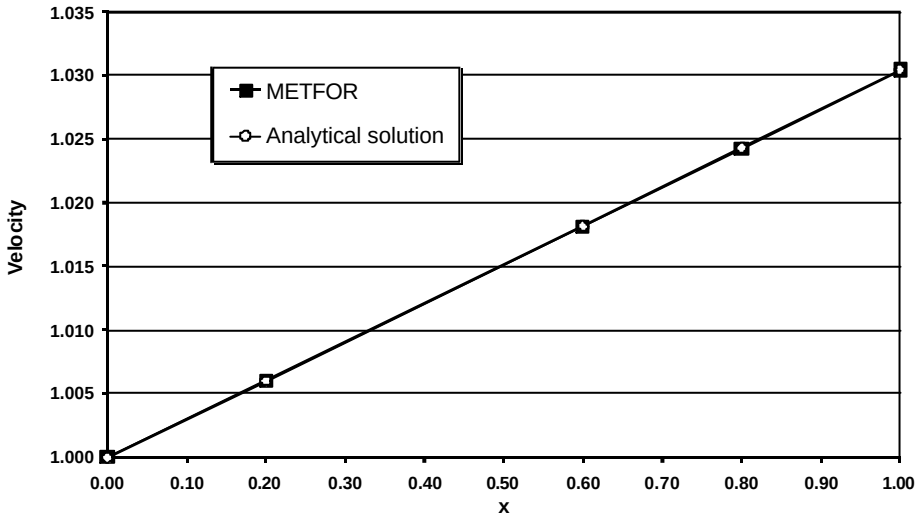

Figure 3: Square section duct with a constant thermal gradient

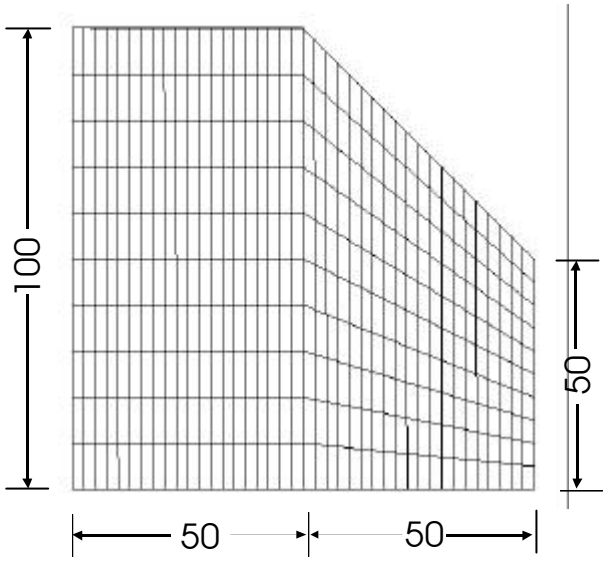

Figure 4: Flow through a nozzle under thermal gradient. Finite element mesh

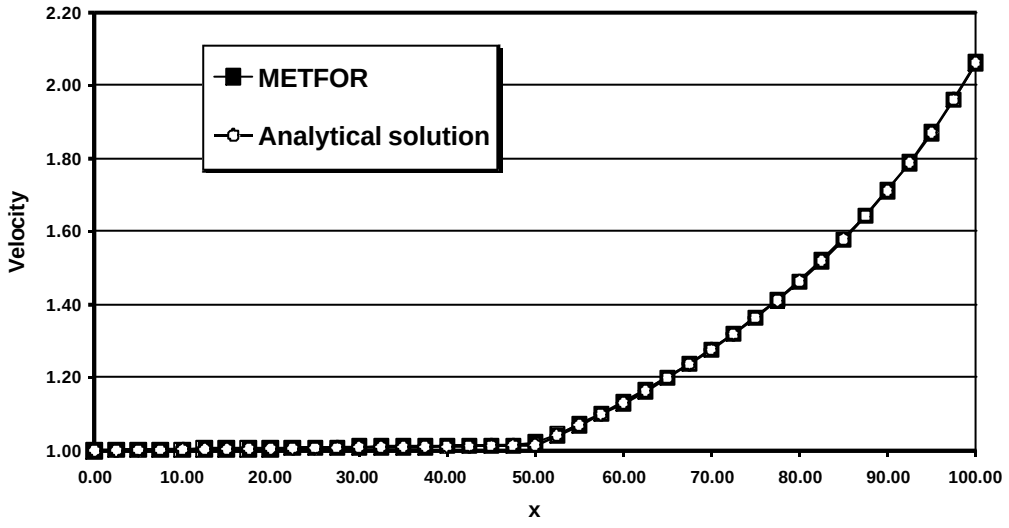

Figure 5: Flow through a nozzle under thermal gradient. Average axial velocity results

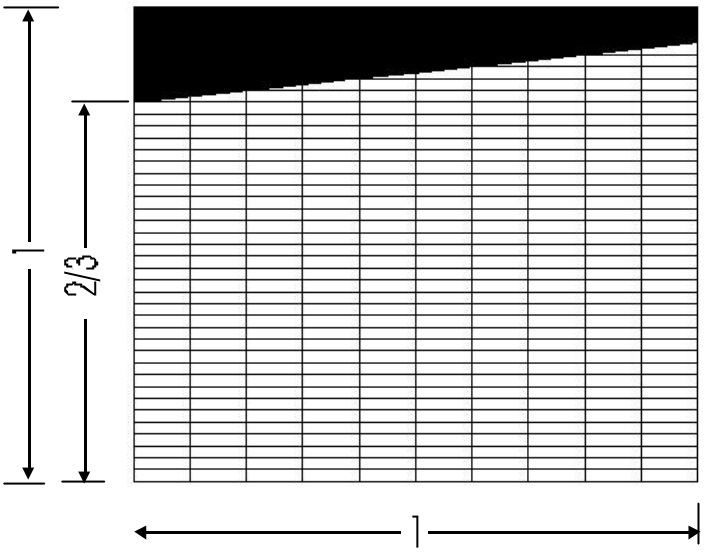

Figure 6: Plane strain plate. Pseudo-concentrations distribution (the grey areas correspond to c<0)

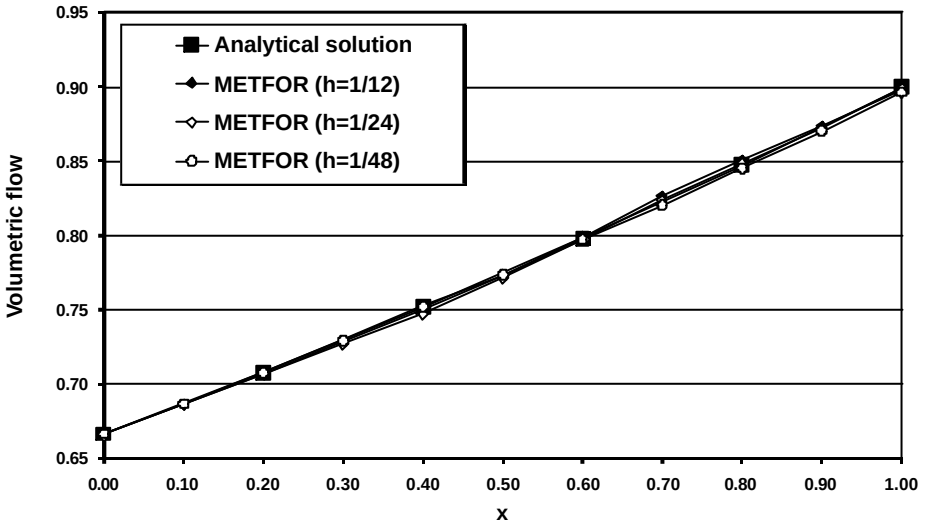

Figure 7: Plane strain plate. Volumetric flow

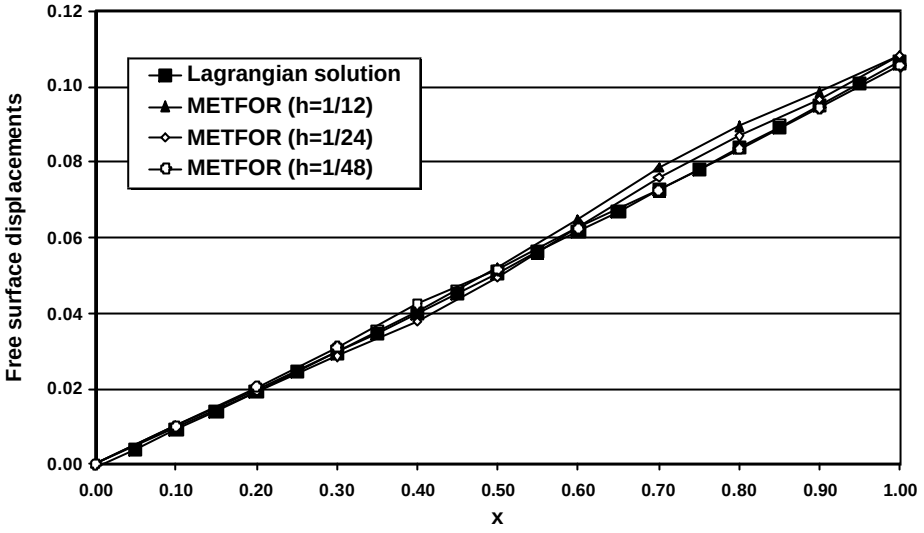

Figure 8: Plane strain plate. Free surface

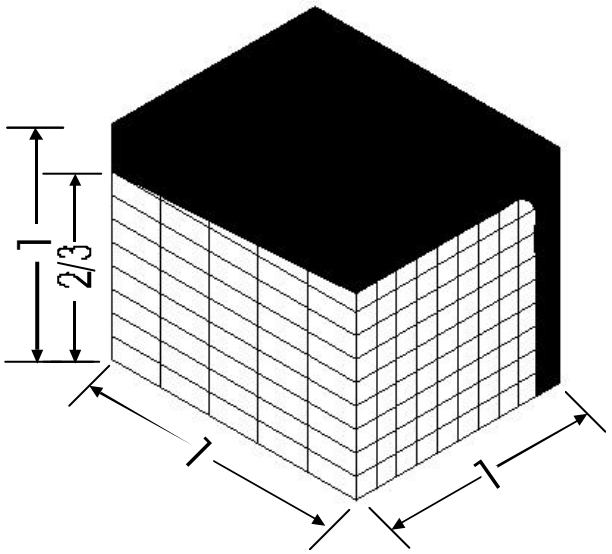

Figure 9: Three-dimensional expansion. The results correspond to the pseudo-concentrations distributions in 1/4 of the problem (the grey areas correspond to c<0)

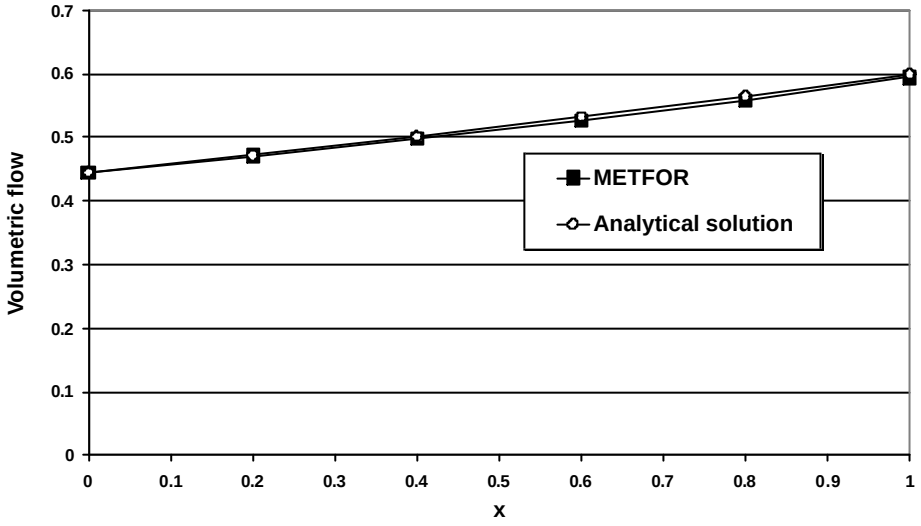

Figure 10: Three dimensional expansion. Volumetric flow